Title

In Vivo Tumor Grading of Prostate Cancer Using Quantitative 111In-Capromab Pendetide SPECT/CT



Journal

Journal of Nuclear Medicine, 51(1)

ISSN

0161-5505

Authors

Seo, Youngho
Aparici, Carina Mari
Cooperberg, Matthew R
et al.

Publication Date

2010

DOI

10.2967/jnumed.109.067108

Peer reviewed

Published in final edited form as:
*J Nucl Med*. 2010 January ; 51(1): 31. doi:10.2967/jnumed.109.067108.

# *In vivo* Tumor Grading of Prostate Cancer using Quantitative $^{111}$In-Capromab Pendetide SPECT/CT

**Youngho Seo, PhD**[1,2,3], **Carina Mari Aparici, MD**[1,4], **Matthew R. Cooperberg, MD**[4,5], **Badrinath R. Konety, MD**[4,5], and **Randall A. Hawkins, MD, PhD**[1,2]

[1]Department of Radiology and Biomedical Imaging, University of California, San Francisco, California

[2]Joint Graduate Group in Bioengineering, University of California, San Francisco and Berkeley, California

[3]Department of Radiation Oncology, Helen Diller Family Comprehensive Cancer Center, University of California, San Francisco, California

[4]San Francisco Veterans Affairs Medical Center, San Francisco, California

[5]Department of Urology, University of California, San Francisco, California

## Abstract

We have developed an *in vivo* antibody uptake quantification method using $^{111}$In-capromab pendetide single photon emission computed tomography combined with computed tomography (SPECT/CT) technology. Our goal is to evaluate this noninvasive antibody quantification method for potential prostate tumor grading.

**Methods—**Our phantom experiments focused on the robustness of an advanced iterative reconstruction algorithm that involves corrections for photon attenuation, scatter, and geometric blurring caused by radionuclide collimators. The conversion factors between image values and tracer concentrations (in Bq/ml) were calculated from uniform phantom filled with aqueous solution of $^{111}InCl_3$ using the same acquisition protocol and reconstruction parameters as for patient studies. In addition, the spatial resolution of the reconstructed images was measured from a point source phantom. The measured spatial resolution was modeled into a point spread function (PSF), and the PSF was implemented in a deconvolution-based partial volume error (PVE) correction algorithm. The recovery capability to correctly estimate true tracer concentration values was tested using prostate-like and bladder-like lesion phantoms fitted in the modified NEMA/IEC body phantom. Patients with biopsy-proven prostate cancer (n=10) who underwent prostatectomy were prospectively enrolled in the preoperative SPECT/CT studies at the San Francisco VA Medical Center. The CT portion of SPECT/CT was used for CT-based attenuation map generation as well as an anatomical localization tool for clinical interpretation. Pathologic Gleason grades were compared with *in vivo* "antibody uptake value" (AUV) normalized by injected dose, effective half-life, and injection-scan time difference. AUVs were calculated in each lobe of prostate gland with cylindrical volumes of interest (VOIs) having dimensions of 1.5 cm both in diameter and height.

**Results—**Reconstructed SPECT images further corrected by the deconvolution-based PVE correction could recover true tracer concentrations in volumes as small as 7.77 ml up to 90% in phantom measurements. From patient studies, there was a statistically significant correlation ($\rho$ =

**Corresponding author:** Youngho Seo, Department of Radiology and Biomedical Imaging, University of California, San Francisco, California 94143-0946. youngho.seo@radiology.ucsf.edu.

0.71, P = 0.033) between higher AUVs (from either left or right lobe) and higher components of pathologic Gleason scores.

**Conclusion—**Our results strongly indicate noninvasive prostate tumor grading potential using quantitative $^{111}$In-capromab pendetide SPECT/CT for prostate cancer evaluation.

### Keywords

prostate cancer; capromab pendetide; SPECT; SPECT/CT; quantification; tracer quantification; quantitative SPECT; prostate specific membrane antigen (PSMA)

## INTRODUCTION

Single photon emission computed tomography (SPECT) and positron emission tomography (PET) are widely used noninvasive molecular imaging tools (1). Although the application of either imaging modality depends on the availability of useful radiotracers, PET always has been preferred when the quantitative accuracy of the result is a particularly important component for a given application (2). In most existing applications, SPECT is less precise primarily because of its lower photon statistics compared to that of PET. In addition, physical correction techniques for photon attenuation, scatter, and geometric blurring caused by radionuclide collimators are not fully implemented or validated in typical SPECT applications (3); thus truly quantitative SPECT for tracer quantification is seldom used.

Out of many potential SPECT applications, the SPECT diagnostic evaluation of prostate cancer metastasis can be greatly enhanced with tracer quantification. $^{111}$In-capromab pendetide is a monoclonal antibody targeting prostate membrane specific antigen (PSMA) labeled with indium-111 that emits high energy photons that are suitable for SPECT imaging (4). Conventional use of $^{111}$In-capromab pendetide SPECT imaging does not require any quantification because the imaging is mainly used to image sites of disease (5).

Immunohistochemical staining with the PSMA-targeting 7E11-C5 monoclonal antibody, the antibody for $^{111}$In-capromab pendetide, has demonstrated more intense staining in malignant prostate tissue than in benign tissue, and also positive staining in lymph node and bony metastases (6). In addition, in specimens obtained from patient studies, the PSMA expression using 7E11-C5 immunohistochemical staining was found to be generally higher in primary cancer and lymph node metastases than in benign epithelium (7). However, *in vivo* PSMA expression using $^{111}$In-capromab pendetide SPECT imaging or any other imaging method has never been correlated with tumor aggressiveness. Conventional use of $^{111}$In-capromab pendetide SPECT imaging has never required any quantification because imaging was mainly used for evaluation of spread of disease (5). To date, however, concerns regarding lack of specificity have limited the widespread clinical applicability of standard $^{111}$In-capromab pendetide-based imaging.

We demonstrate how tracer quantification through quantitative SPECT enables the correlation between *in vivo* PSMA expression as determined from imaging and pathologic tumor grade. Our approaches to tracer quantification are primarily focused on the combined SPECT/computed tomography (CT) technology (8) which provides practical procedures for photon attenuation correction of $^{111}$In data (9). We also used corrections for photon scatter and geometric blurring caused by radionuclide collimators for SPECT image reconstruction (9-11). Our approach is in line with some of previous efforts using CT-based corrections in iterative SPECT reconstruction algorithms to obtain better quantitative accuracies of reconstructed concentrations in comparison to correction methods based on SPECT transmission scans (12). In particular, it must be noted that correct implementation of attenuation correction was found to be a significant factor to achieve artifacts-free SPECT

images (13) and improved quantitative information of radioactivity distribution (14). However, with regards to tracer quantification within small volumes of interest (e.g., prostate glands), we further utilized additional post-reconstruction partial volume technique we originally developed for positron emission tomography images to achieve improved quantitative information of tracer concentrations (15). As a result, after careful phantom calibration evaluations, we were able to convert pixel values in SPECT reconstructed volumes into tracer concentration values (Bq/ml). Using the tracer concentration values normalized by appropriate patient-specific imaging variables such as injected dose and time interval between injection and scan times, the correlation of *in vivo* PSMA expression was evaluated with pathologic tumor grade from prospectively enrolled prostate cancer patients who underwent radical prostatectomy following the SPECT/CT imaging.

## MATERIALS AND METHODS

### SPECT/CT acquisition and reconstruction parameters

All of our studies utilized a commercially available SPECT/CT scanner (Precedence SPECT/CT with 3/8″ NaI(Tl) and 16 slice multidetector CT, Philips Healthcare, Andover, MA) installed at San Francisco Veterans Affairs Medical Center (SFVAMC). All SPECT data in both phantom and patient studies were acquired using a 128×128 matrix with a 4.664 mm pixel size using medium energy general purpose (MEGP) collimators. The SPECT acquisition was performed with 64 stops (128 angles by two camera heads) at 55 seconds per stop for a 360° rotation. SPECT reconstructions were performed using an algorithm involving CT-based attenuation correction, and scatter and geometric blurring corrections (Astonish, Philips Healthcare) with 12 iterations and 8 subsets of OSEM. The postfilter of reconstructed images was Hanning with 1.5 cutoff frequency. In case there was a visual mismatch between CT attenuation map and the SPECT emission data, a manual registration of the two data was performed before proceeded to reconstruct the final SPECT images. Using the JETStream workstation provided by the scanner manufacturer, each SPECT reconstruction took approximately 30 minutes each. For patient studies, approximately 5 mCi of $^{111}$In-capromab pendetide was administered intravenously, and followed by the SPECT/CT acquisitions at approximately 96 hours postinjection. The helical xray CT was performed without iodinated contrast agent using the manufacturer's default CT attenuation correction acquisition parameters. The CT data were reconstructed using a filtered back-projection algorithm provided by the scanner manufacturer.

### Phantom preparations

In order to calculate radiotracer concentrations (Bq/ml) in each voxel of SPECT reconstructed volumes, we performed a SPECT/CT scan of phantoms that are divided into three parts: 1) uniform volume, 2) point source, and 3) small and large volumetric lesions. All three parts of the phantoms were fit within one SPECT field of view (FOV) to minimize the number of scans needed to be performed. The uniform volume filled with aqueous solution of $^{111}InCl_3$ (53.65 MBq) was needed to test uniformity of the reconstructed SPECT image, and to calculate a conversion factor from voxel values (arbitrary unit) to radiotracer concentrations (Bq/ml). This uniform volume was only partially filled to ensure a complete mixing of the $^{111}InCl_3$ aqueous solution. The point source was simulated using a drop of $^{111}InCl_3$ solution within a small centrifuge tube. This point source was used to measure the spatial resolution of reconstructed SPECT images. The point spread function was estimated from the spatial resolution value, and was an input parameter to the previously developed post-reconstruction partial volume error (PVE) correction algorithm (15,16). This PVE correction algorithm iteratively compensates partial volume errors of spill-ins and spill-outs from neighboring pixels by deconvolving reconstructed volume with the measured point spread function. The small and large lesions

were simulated in phantoms as for prostate gland and bladder, and to test our physical correction techniques and PVE correction algorithm to recover known tracer concentration values.

The modified NEMA/IEC body phantom to include bladder-like (146 ml) and prostate-like (7.77 ml) lesions filled with $^{111}InCl_3$ aqueous solution was prepared in the radiopharmacy laboratory at SFVAMC. At scan time, activity concentrations for the bladder-like and prostate-like lesions were 32.9 kBq/ml and 636.3 kBq/ml, respectively. The rest of the parts in the body phantom, the body part and the six spheres were filled with nonradioactive water to simulate attenuation medium. All dose measurements before phantom filling were conducted using a dose calibrator calibrated for $^{111}In$. Once the radioactivity is filled within the phantom compartments, agitation of the phantom with leak-proof covers and screws fastened was performed to ensure complete mixing of $^{111}InCl_3$ with water at room temperature. The bladder-like and prostate-like lesions were manufactured in the investigator's own machine shop at the University of California, San Francisco, and were fit in the standard NEMA/IEC body phantom (17).

### Patient recruitment and pathologic analysis

Patient subjects were recruited following an institutional review board (IRB) approved protocol for collecting image data and other test results related to the imaging studies including descriptive pathologic evaluation after prostatectomy. Other than the eligibility of prostatectomy, no other restrictive patient selection criteria were imposed.

### Advanced reconstruction and deconvolution techniques on patient images

We focused on tracer quantification in small volumes like the prostate gland. In addition, as far as the spatial resolution of the $^{111}In$-SPECT/CT imaging allows, our goal is to develop quantitative indices for each lobe of the prostate gland. Given the often multicentric distribution of prostate cancer in the gland, even left/right quantitative indices should be useful in characterizing disease. Our choice of reconstruction parameters was based on a preliminary study where an extra correction term such as attenuation correction in an iterative reconstruction algorithm requires typically twice the iterations to maintain the same signal-to-noise ratio before and after inclusion of the extra correction term(10). Therefore, including CT-based photon attenuation correction and geometric blurring correction as well as scatter correction, we chose 12 iterations, which are 6 times the manufacturer's default number of 2 iterations of OSEM algorithm when these three correction terms are not included. This advanced reconstruction algorithm was necessary to present good image quality for interpretation of $^{111}In$-capromab pendetide SPECT/CT studies. The measured spatial resolution was an average of 9 mm FWHM.

However, for tracer quantification within the prostate gland, our volumes of interest (VOIs) were two identical cylinders having dimensions of 1.5 cm both in diameter and height at each side of the prostate gland. The VOI size was smaller than twice the size of FWHM. Our deconvolution-based post-reconstruction PVE correction was necessary to further tighten the errors associated with tracer concentration value estimates. Figure 1 illustrates this tightening effect visually. The top images are prior to the application of the deconvolution-based PVE correction in transaxial and coronal views; the bottom images are after the PVE correction.

### Antibody Uptake Value correlation with tumor grade

The cylindrical VOIs were drawn completely within each lobe of prostate gland to calculate mean value of tracer concentrations in the unit of Bq/ml. The tracer concentration values were converted to “Antibody Uptake Value” (AUV) which is similar to Standardized Uptake Value (SUV) (18) commonly used in PET quantitation except the AUV is not normalized by individual patient weight because *in vivo* uptake of antibody such as 7E11-C5 in $^{111}In$-

capromab pendetide is a biochemical characteristic at the level of tissue, which should not have significant variance depending on the patient weight. AUVs were calculated from the prospectively enrolled 10 preoperative patient data using the following formula:

$$\mathrm{AUV}\,[\mathrm{Bq/ml/MBq}] = \frac{C'(t_s)\cdot e^{\lambda_e \quad f\left(t_f \quad -t_i\right)}}{A(t_i)} \qquad \text{Eq. 1}$$

where $C'(t_s)$ is activity concentration (Bq/ml) estimated using the conversion factor from the uniformity measurement, and corrected with the 9 mm FWHM iterative deconvolution algorithm, $\lambda_{eff}$ is effective decay constant of $^{111}$In-capromab pendetide (=0.01034 $h^{-1}$), $t_s$ is the scan time, $t_i$ is the injection time (in h), and $A(t_i)$ is the total activity injected (in MBq). The unit of AUV is selected as Bq/ml/MBq because this unit provides a user-friendly range of values typically between 20 and 100.

After these AUVs were calculated from patients who went through radical prostatectomy and anatomic pathology after the surgical procedure, we obtained pathologic tumor grades from all of these patients. The pathologic Gleason score is often a valuable prognostic factor in prostate cancer management (19). The Gleason grading system assigns a grade from 1 (very well differentiated) to 5 (very poorly differentiated) to the most dominant and second dominant histological patterns (20). Comparison was made between higher AUVs (either left lobe or right lobe) and higher grade of the Gleason score because given the limitations of the imaging test in terms of not having finer spatial resolution, smaller segmentation of AUV measurements is difficult to justify. The higher grade of the Gleason score was chosen assuming high AUV can be closely related to intensive PSMA overexpression. As shown in Figure 2, the higher Gleason grade from our 10 patient data sets was either 3 (from 3+3 Gleason score) or 4 (either from 3+4 or from 4+3).

## RESULTS

### $^{111}$In concentration calculation from small volumes

The uniform volume after reconstruction using iterative ordered subsets expectation maximization (OSEM) algorithm that involved CT-based attenuation correction, scatter and geometric blurring corrections, resulted in a SPECT reconstructed image that showed uniform line profiles shown in Figure 3. This line profile was obtained from a transaxial slice stacked over 20 uniform slices. From this measurement, the conversion factors as multiplication factors from the reconstructed image value (arbitrary unit) to the activity concentration (Bq/ml) were estimated at 9.87 and 13.31 for PVE-uncorrected images and PVE-corrected images, respectively. The reconstructed point source image resulted in an average full width half maximum (FWHM) of 9 mm using Gaussian function fits in all 3 Cartesian coordinates. The average FWHM value was a mean value of three FWHMs corresponding to three Cartesian coordinates. Thus, after applying the 9 mm FWHM point spread function to our iterative deconvolution technique to correct for partial volume errors as well as the conversion factor from the uniform phantom above, we could recover activity concentrations (in Bq/ml) up to approximately 90% of true values in a small prostate-like lesion (7.77 ml) and up to almost 100% of true values in a large bladder-like lesion (146 ml). Figure 4 shows that our PVE correction technique outperforms non-PVE correction conversion method in the concentration value recovery process.

### SPECTCT images of patients after advanced corrective reconstruction

Figure 1 illustrates this tightening effect visually. This visual effect is an example of how the deconvolution-based PVE correction algorithm was necessary to quantify a small volume such

as the prostate gland because even the reconstruction algorithm that incorporated photon attenuation, scatter, and collimator response corrections was not sufficient to provide the necessary spatial resolution that can be used to draw values in small VOIs. It should be also noted that the blurring of the tracer distribution in the prostate gland was significantly improved after the PVE correction was applied.

### Antibody Uptake Value correlation with tumor grade

Figure 2 shows the correlations between AUVs and Gleason grades of tumors. As indicated in Figure 2, the deconvolution-based PVE correction provides a statistically more significant correlation between the two values, which could result in the potential use of $^{111}$In-capromab pendetide SPECT/CT as an *in vivo* tumor grading tool. The Spearman's rank correlation test shows that correlation coefficients were $\rho = 0.64$ and 0.71, respectively for Gleason tumor grade correlation with PVE-uncorrected AUVs and with PVE-corrected AUVs. The two-sided P values were 0.055 and 0.033, respectively. Hence, if we consider the statistical significance with $P < 0.05$, the deconvolution-based PVE correction needs to be used to make the correlation results statistically significant using our limited sample size (n=10).

## DISCUSSION

The conversion factor method to calculate estimated activity concentration values in the unit of Bq/ml is routinely applied in PET; but has not been widely adopted in SPECT this scheme yet primarily because of worse photon statistics and difficulties in applying necessary physical corrections. We report validation of a novel approach involving correction factors for three major physical perturbations (photon attenuation, scatter, geometric blurring caused by radionuclide collimators) for SPECT imaging. These physical correction techniques provide a higher target-to-background ratio (21). Therefore, even if the physical detection efficiency is not improved, an indirect improvement in photon statistics with the iterative reconstruction algorithm is achieved. Dual-modality SPECT/CT technology results in improved SPECT quantification, particularly with regards to photon attenuation correction.

As we have shown in our report, tracer quantification that is correlative with biological signatures of tissue such as PSMA expression for prostate cancer also requires careful thought process on normalization methods to minimize inter-patient variability. In the future, we plan to not only accumulate more patient data and a wider range of Gleason tumor grade at least to capture some of grade 5 components, but also explore some other ways to evaluate the data correlation with other biological features of prostate cancer such as spectroscopic biomarkers of the cancer that can be obtained from magnetic resonance spectroscopic imaging combined with magnetic resonance imaging (MRSI/MRI) (22).

The extension of tracer quantification in distant metastatic sites is another possibility if we can have access to them for pathologic evaluations. The same analysis we have developed in this report can be performed to compare *in vivo* antibody uptake value and pathologic tumor status. Eventually, our long term goal is to develop a validated preoperative imaging-based tumor staging and grading system to alleviate the problems of understaging on prostate biopsy, which complicate prostate cancer decision-making, leading to both under- and over-treatment of localized disease. There exists a great need for continuous investigation of the novel radiotracers for prostate cancer which specifically target promising biomarkers such as PSMA such as the one reported by Hiller SM et al. (23). We hope our results will thus help invigorate the adoption of quantitative SPECT imaging techniques using these newer tracers.

Gleason score has been considered as a predictor of prostate cancer mortality (24). However, it was only recent to find that the mortality rates differ among patients with a Gleason score of 7 depending on whether Gleason pattern 4 is primary or secondary. For example, Tollefson

MK et al. reported that patients with primary Gleason grade 4 (thus, Gleason score of 4+3) have higher rates of biochemical failure, systemic recurrence, and mortality from the disease than those with primary Gleason grade 3 (thus, Gleason score of 3+4) (25). In our current study, we did not distinguish these two different patterns of Gleason score mainly due to the limited spatial resolution of SPECT even after advanced reconstruction algorithms and partial volume error correction techniques were used as shown in this manuscript. When we find out ways to improve the spatial resolution further in the future, the different patterns of the Gleason score of 7 will be evaluated.

## CONCLUSION

We performed phantom and patient studies for quantitative $^{111}$In-capromab pendetide SPECT imaging using a commercially available SPECT/CT scanner with advanced SPECT reconstruction algorithm and partial volume correction technique to quantify radiolabeled antibody concentrations *in vivo*. Our results indicate noninvasive prostate tumor grading potential using quantitative $^{111}$In-capromab pendetide SPECT/CT for prostate cancer evaluation. This conclusion will be followed carefully with an expanded patient population including patients possessing Gleason grades lower than 3 and higher than 4, both of which are not included in the presented study. In addition, the differences between the primary and secondary Gleason patterns will be examined in the future studies.

## Acknowledgments

We thank Marilyn Morrissey and Charisa Thomas at the San Francisco Veterans Affairs Medical Center for their technical assistance for the imaging studies performed for this report. Y.S. was partially funded by National Cancer Institute Grant #5 K25 CA114254. C.M.A. was partially supported by the University of California Industry-University Cooperative Research Program Grant dig 06-10210 with Philips Healthcare.

## REFERENCES

1. Jansen FP, Vanderheyden JL. The future of SPECT in a time of PET. Nucl Med Biol 2007;34:733–735. [PubMed: 17921025]
2. Flux G, Bardies M, Monsieurs M, Savolainen S, Strands SE, Lassmann M. The impact of PET and SPECT on dosimetry for targeted radionuclide therapy. Z Med Phys 2006;16:47–59. [PubMed: 16696370]
3. Garcia EV. SPECT attenuation correction: an essential tool to realize nuclear cardiology's manifest destiny. J Nucl Cardiol 2007;14:16–24. [PubMed: 17276302]
4. Manyak MJ. Indium-111 capromab pendetide in the management of recurrent prostate cancer. Expert Rev Anticancer Ther 2008;8:175–181. [PubMed: 18279057]
5. Nagda SN, Mohideen N, Lo SS, Khan U, Dillehay G, Wagner R, Campbell S, Flanigan R. Long-term follow-up of 111In-capromab pendetide (ProstaScint) scan as pretreatment assessment in patients who undergo salvage radiotherapy for rising prostate-specific antigen after radical prostatectomy for prostate cancer. Int J Radiat Oncol Biol Phys 2007;67:834–840. [PubMed: 17293236]
6. Fair WR, Israeli RS, Heston WD. Prostate-specific membrane antigen. Prostate 1997;32:140–148. [PubMed: 9215402]
7. Sweat SD, Pacelli A, Murphy GP, Bostwick DG. Prostate-specific membrane antigen expression is greatest in prostate adenocarcinoma and lymph node metastases. Urology 1998;52:637–640. [PubMed: 9763084]
8. Seo Y, Mari C, Hasegawa BH. Technological development and advances in single-photon emission computed tomography/computed tomography. Semin Nucl Med 2008;38:177–198. [PubMed: 18396178]
9. Seo Y, Wong KH, Hasegawa BH. Calculation and validation of the use of effective attenuation correction for attenuation correction in In-111 SPECT. Med Phys 2005;32:3628–3635. [PubMed: 16475761]

10. Seo Y, Wong KH, Sun M, Franc BL, Hawkins RA, Hasegawa BH. Correction of photon attenuation and collimator response for a body-contouring SPECT/CT imaging system. J Nucl Med 2005;46:868–877. [PubMed: 15872362]
11. Song X, Segars WP, Du Y, Tsui BM, Frey EC. Fast modelling of the collimator-detector response in Monte Carlo simulation of SPECT imaging using the angular response function. Phys Med Biol 2005;50:1791–1804. [PubMed: 15815096]
12. Vandervoort E, Celler A, Harrop R. Implementation of an iterative scatter correction, the influence of attenuation map quality and their effect on absolute quantitation in SPECT. Phys Med Biol 2007;52:1527–1545. [PubMed: 17301469]
13. Celler A, Dixon KL, Chang Z, Blinder S, Powe J, Harrop R. Problems created in attenuation-corrected SPECT images by artifacts in attenuation maps: a simulation study. J Nucl Med 2005;46:335–343. [PubMed: 15695795]
14. Tsui BM, Gullberg GT, Edgerton ER, Ballard JG, Perry JR, McCartney WH, Berg J. Correction of nonuniform attenuation in cardiac SPECT imaging. J Nucl Med 1989;30:497–507. [PubMed: 2786944]
15. Teo BK, Seo Y, Bacharach SL, et al. Partial-volume correction in PET: validation of an iterative postreconstruction method with phantom and patient data. J Nucl Med 2007;48:802–810. [PubMed: 17475970]
16. Soret M, Bacharach SL, Buvat I. Partial-volume effect in PET tumor imaging. J Nucl Med 2007;48:932–945. [PubMed: 17504879]
17. Seo Y. Prostate-bladder phantom for radionuclide imaging research. Nuclear Science Symposium Conference Record, 2008 NSS '08 IEEE 2009:4820–4822.
18. Huang SC. Anatomy of SUV. Standardized uptake value. Nucl Med Biol 2000;27:643–646. [PubMed: 11091106]
19. Zakian KL, Sircar K, Hricak H, et al. Correlation of proton MR spectroscopic imaging with gleason score based on step-section pathologic analysis after radical prostatectomy. Radiology 2005;234:804–814. [PubMed: 15734935]
20. Gleason DF. Histologic grading of prostate cancer: a perspective. Hum Pathol 1992;23:273–279. [PubMed: 1555838]
21. Seo Y, Franc BL, Hawkins RA, Wong KH, Hasegawa BH. Progress in SPECT/CT imaging of prostate cancer. Technol Cancer Res Treat 2006;5:329–336. [PubMed: 16866563]
22. Swanson MG, Vigneron DB, Tran TK, Kurhanewicz J. Magnetic resonance imaging and spectroscopic imaging of prostate cancer. Cancer Invest 2001;19:510–523. [PubMed: 11458818]
23. Hillier SM, Maresca KP, Femia FJ, et al. Preclinical evaluation of novel glutamate-urealysine analogues that target prostate-specific membrane antigen as molecular imaging pharmaceuticals for prostate cancer. Cancer Res 2009;69:6932–6940. [PubMed: 19706750]
24. Andren O, Fall K, Franzen L, Andersson SO, Johansson JE, Rubin MA. How well does the Gleason score predict prostate cancer death? A 20-year followup of a population based cohort in Sweden. J Urol 2006;175:1337–1340. [PubMed: 16515993]
25. Tollefson MK, Leibovich BC, Slezak JM, Zincke H, Blute ML. Long-term prognostic significance of primary Gleason pattern in patients with Gleason score 7 prostate cancer: impact on prostate cancer specific survival. J Urol 2006;175:547–551. [PubMed: 16406993]

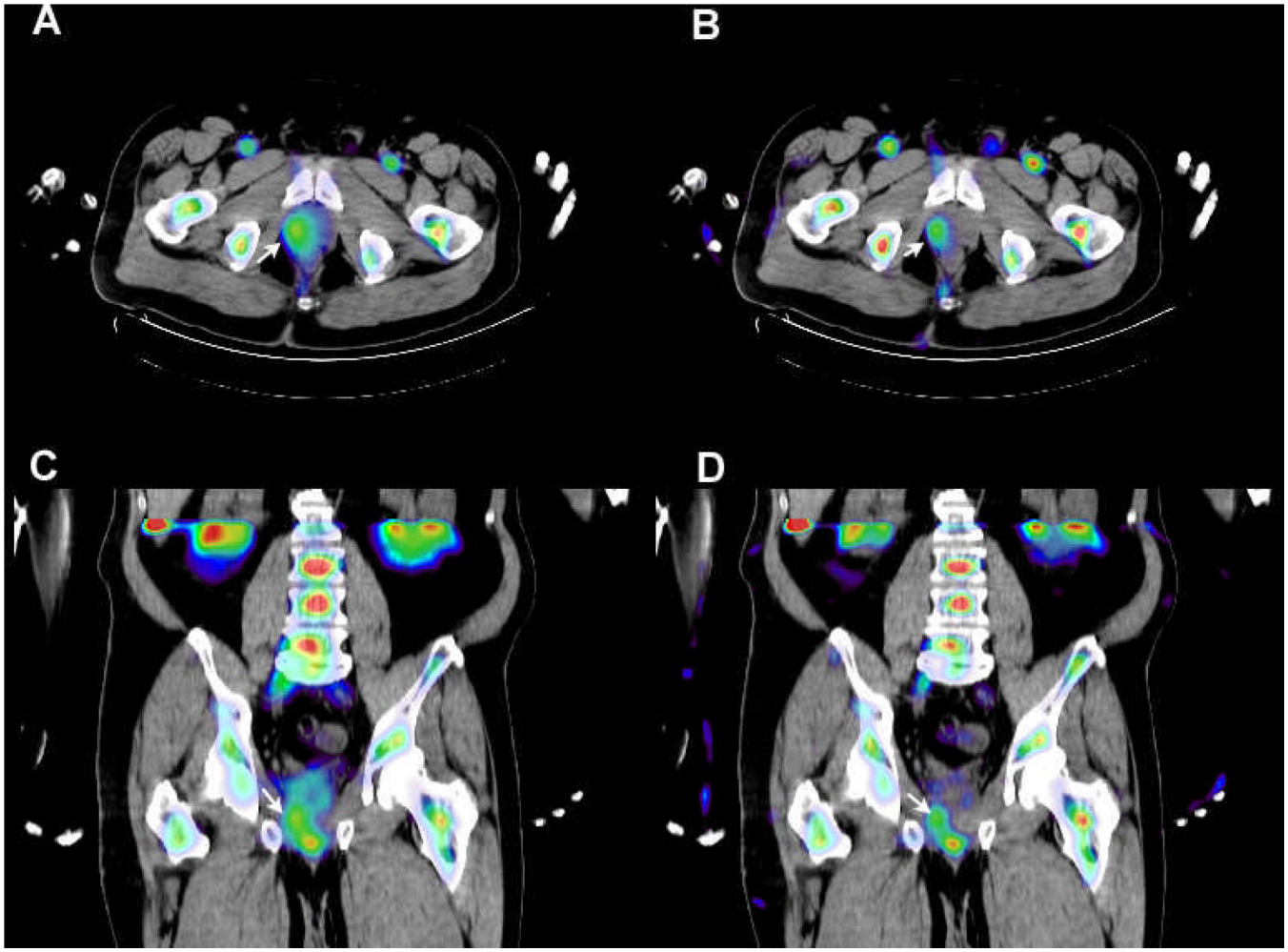


**Figure 1.**
The effect of deconvolution-based partial volume error correction on reconstructed SPECT/CT images. (A) and (C) are before correction (left column) and (B) and (D) are after the PVE correction. The transaxial (top row) and coronal (bottom row) views are shown. White arrows indicate areas of the uptake patterns (the prostate gland), showing improved spatial resolution after the PVE correction.

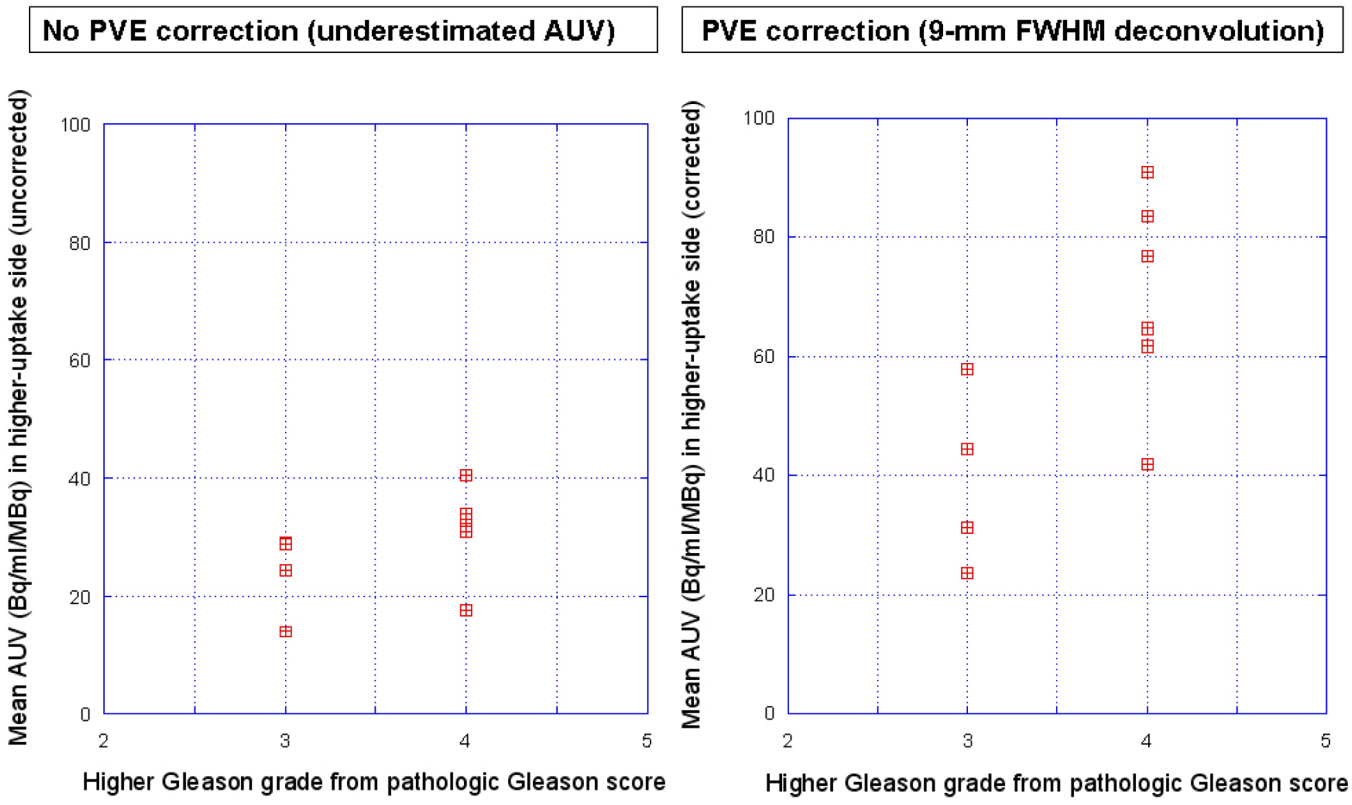


**Figure 2.**

Correlation plots of AUVs against Gleason tumor grades from 10 patient data. All patients went through preoperative SPECT/CT imaging of $^{111}$In-capromab pendetide and prostatectomies. Gleason tumor grades were obtained from anatomical pathology of the prostatectomies. AUVs were calculated before and after the deconvolution-based PVE correction was applied.

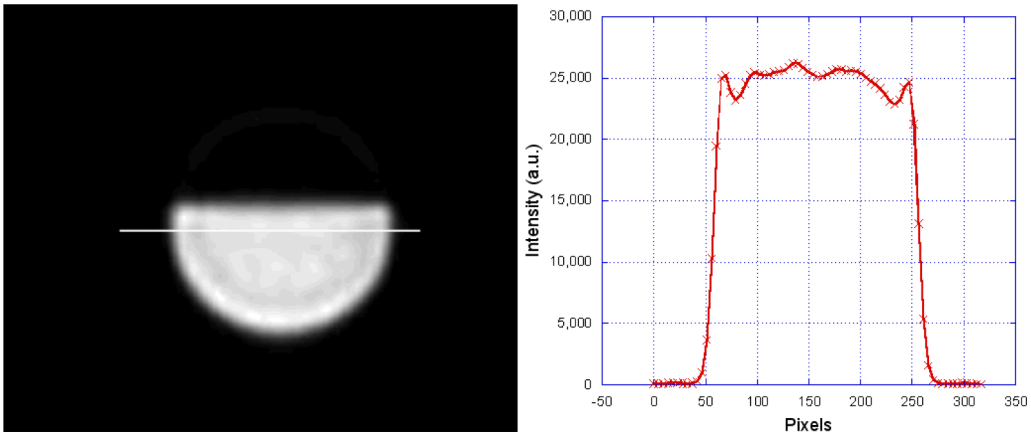


**Figure 3.**

Reconstructed uniform phantom image in transaxial view. The phantom was in cylindrical shape, and aqueous solution of $^{111}InCl_3$ was mixed with water, and filled in the cylindrical volume partially to ensure a complete mixing with water. The line profile shows a fairly uniform intensity pattern except small dips near the edge close to the wall.

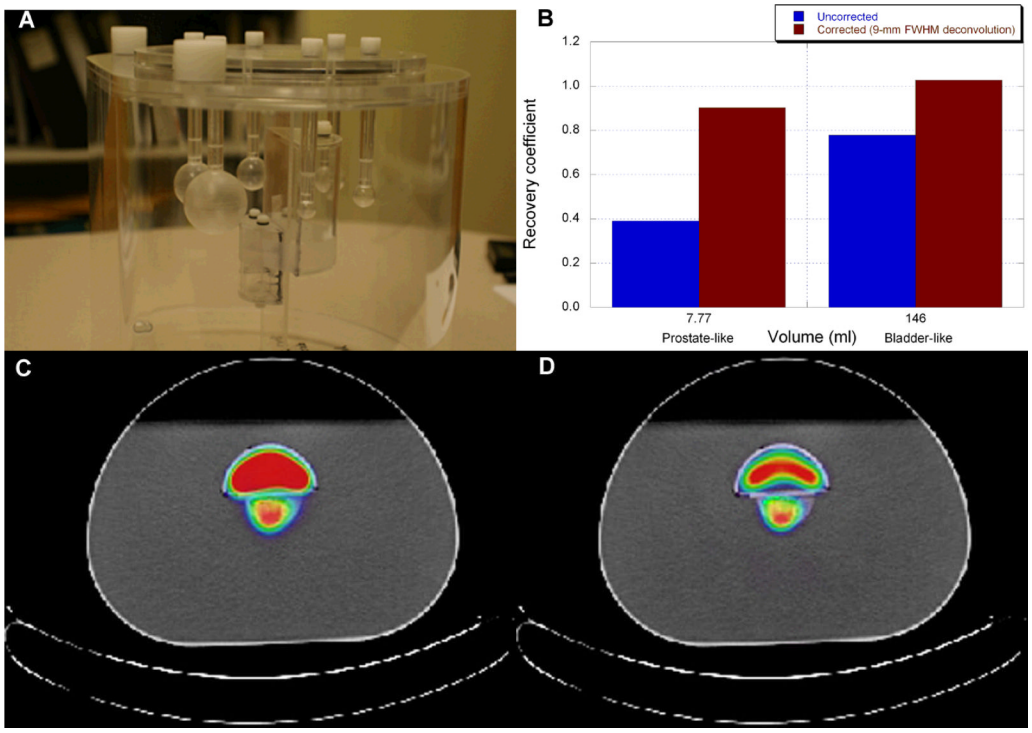


**Figure 4.**

Recovery coefficients were measured using a modified NEMA/IEC body phantom that contains multiple prostate lesions (7.77 ml the smallest) and bladder lesion (146 ml). (A) A photograph of the modified NEMA/IEC body phantom. (B) The chart that compares recovery coefficients in reconstructed images with and without PVE correction. The deconvolution-corrected measurement recovers tracer concentrations significantly even in a very small volume (7.77 ml), while the deconvolution correction effect is less significant in a large lesion (146 ml). Reconstructed phantom image slices (transaxial view showing the two filled lesions) uncorrected (C) and corrected (D) by the PVE correction algorithm are also shown.